JOURNAL OF MATAERIALS SCIENCE 29 (1994) 693–699

Analysis of flexural creep for an SiC fibre-reinforced Si_3N_4 composite

R. B. THAYER J.-M. YANG
Department of Materials Science and Engineering, University of California, Los Angeles, CA 90024-1595, USA

A numerical analysis for extracting the tensile and compressive creep power-law parameters from flexural test data is applied to an SiC fibre-reinforced hot-pressed Si_3N_4 composite. The evolution and steady-state conditions of the stress distribution during creep and the effect of neutral-plane migration on the creep behaviour are also analysed. Finally, the kinetics and mechanisms of high-temperature creep in the composite are discussed with respect to the results of the numerical analysis.

1. Introduction

Continuous fibre-reinforced ceramic matrix composites are promising engineering materials for high-temperature structural applications such as gas turbine engines [1, 2]. Before these composites can be reliably used in structural applications at elevated temperatures, a greater understanding of their creep characteristics and mechanisms must be developed. Up to now, the majority of creep tests have been conducted using three-point and four-point flexural tests. This is primarily due to the simplicity of specimen geometry and experimental procedures. The major drawback in using this technique is the complex stress distribution that develops during testing. When analysing the power-law creep parameters from bend test data, it is usually assumed that tensile and compressive creep obey the same constitutive law and only one stress exponent is determined to characterize the material. Experimentally, though, tensile and compressive creep have been found to be different in siliconized SiC [3], Al_2O_3 and Si_3N_4 [4], as well as in most ceramic materials [5]. In flexural creep, differences in tensile and compressive steady-state strain rates and stress exponents result in a non-linear stress dependence.

Recently, the creep behaviour of an SiC fibre-reinforced hot-pressed Si_3N_4 composite (with 5 wt % Y_2O_3 and 1.25 wt % MgO as sintering additives) has been characterized using the four-point bending test. Typical creep responses of the 20 vol % composite tested at different temperatures and stresses are shown in Figs 1 and 2, respectively [6, 7]. The purpose of this study is to conduct a numerical analysis for extracting both tensile and compressive creep power-law parameters from bend test data. The numerical scheme developed by Chuang [8] is used in the pressent study. Consistent agreement between the experimentally measured results and those determined numerically from the governing equations from this analysis has been reported for SiAlON [9] and Nicalon fabric-reinforced SiC composite [10]. The implications of these parameters for the creep behaviour of the composites will also be discussed.

2. Numerical analysis

To accommodate both compressive and tensile creep in a flexing bar, the Norton power law [11] for creep is expressed as

$$\dot{\varepsilon} = A_i\left(\frac{\sigma}{\sigma_0}\right)^{n_i} \tag{1}$$

where σ_0 is a constant with dimensions of stress, and the subscript i is either t or c to indicate tension or compression, respectively. Invoking Bernoulli's hypothesis that plane sections remain plane in bending, the strain of an element, ε, a distance Y from the neutral plane is $\varepsilon = KY$, where K is the curvature of the neutral plane. The strain rate of a beam element is given by $\dot{\varepsilon} = \dot{K}Y + K\dot{Y}$, but because the neutral-plane migration during steady-state creep is negligible, the $K\dot{Y}$ term is dropped. The stress in an element of the beam a distance Y from the neutral plane is then given by

$$\sigma = \sigma_0\left(\frac{\dot{K}Y}{A_i}\right)^{1/n_i} = \sigma_0\left(\frac{\dot{k}y}{A_i}\right)^{1/n_i} \tag{2}$$

Here, $\dot{k} = \dot{K}H$ and $y = Y/H$ where H is the full beam height. Using Equation 2 to derive the equilibrium conditions, ΣF_x (force balance) = 0 and ΣM (moment balance) = 0, for a bar in flexural creep resulted in two governing equations which are given in the Appendix. Because no analytic solutions were found for determining n_c, n_t, A_c and A_t from the two governing equations, a numerical approach was developed to find solutions. The methods used are summarized in the Appendix with more detailed descriptions available elsewhere [8, 9]. Once the power-law parameters for a material have been numerically determined, stress distributions over the height of the beam may be calculated for a set of test conditions.

0022–2461

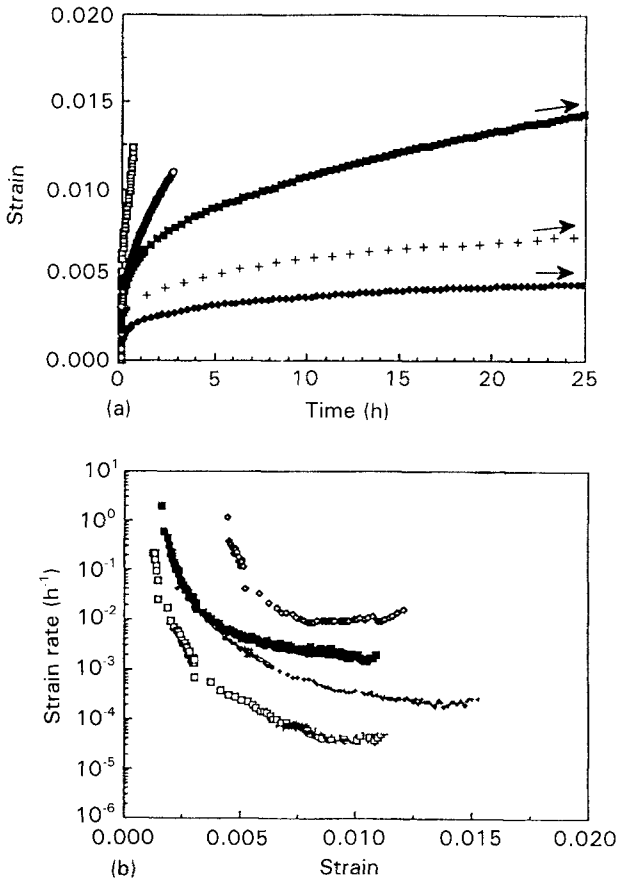

Figure 1 Creep response for 20 vol % composite at 250 MPa and various temperatures. (a) Creep strain versus time: (◆) 1200 °C, (+) 1275 °C, (■) 1350 °C, (○) 1390 °C, (□) 1450 °C, (b) Creep strain-rate versus creep strain: (□) 1275 °C, (+) 1350 °C, (■) 1390 °C, (◇) 1425 °C.

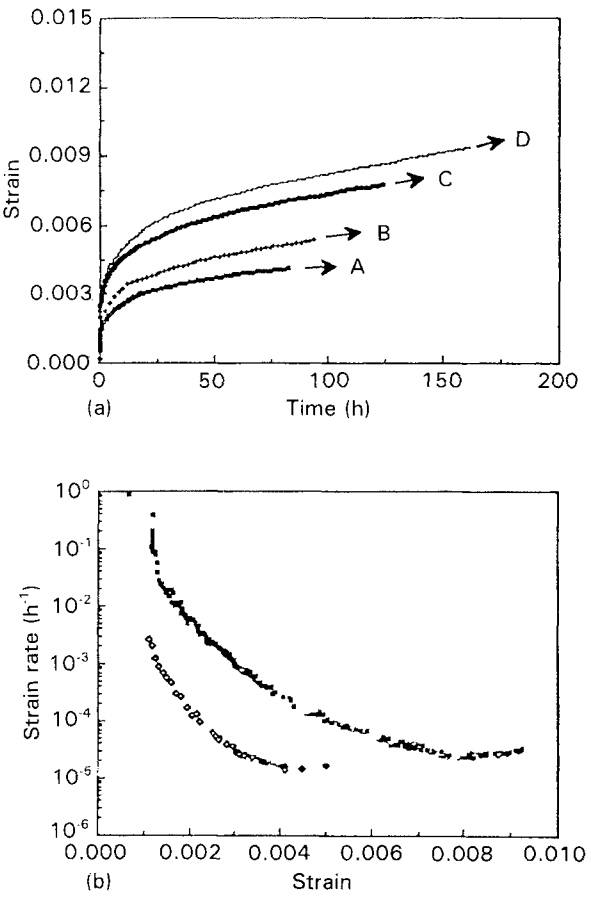

Figure 2 Creep response for 20 vol% composite at 1200 °C and various stresses. (a) Creep strain versus time: (A) 250 MPa, (B) 280 MPa, (C) 330 MPa, (D) 350 MPa. (b) Creep strain-rate versus creep strain: (◇) 250 MPa, (■) 350 MPa.

3. Results

3.1. Tensile and compressive stress exponents

Steady-state creep relationships obtained from the flexural creep tests [7] were fitted by using the numerical procedure outlined above and in the Appendix. The solutions, plotted as normalized curvature rate versus normalized moment, are shown in Fig. 3 for the unreinforced Si_3N_4 and for the 20 and 30 vol % fibre composites. Power-law parameters determined from the best-fit solutions are tabulated in Table I. The results clearly indicate a profound difference between tensile and compressive creep in the matrix Si_3N_4. In the composites, smaller differences were estimated between the tensile and compressive creep behaviour, i.e. the behaviour was less non-linear. In fact, when compared only on the basis of a regression fit, the general curve fit of the limited composite data was only a slight improvement over the linear fit. Obviously, data taken over a larger stress range would narrow the confidence interval of the fit and thus the stress parameters. The conventional linear regression exponents given elsewhere [7] ($n = 2.5$ for both composites) are approximately averages of the tensile and compressive creep stress exponents determined numerically [8].

TABLE I Tensile and compressive power-law parameters from creep in four-point bending

Material	A_t	n_t	A_c	n_c
Monolithic Si_3N_4	6.00×10^{-11}	22	5.50×10^{-9}	0.41
20 vol % composite	7.50×10^{-11}	5	4.00×10^{-10}	1.1
30 vol % composite	1.25×10^{-13}	5	5.50×10^{-10}	0.70

3.2. Neutral plane and stress distribution

In estimating the power-law parameters determining the strain rate–applied moment relationship, a set of values of neutral plane coordinates (NPC) locating the neutral plane with respect to the compressive surface (h_c) for each strain rate was calculated. Plotted in Fig. 4 is the normalized neutral-plane location versus the applied moment normalized using an arbitrary value of stress. The neutral-plane location is found to have a stronger dependence on the applied moment in the matrix specimens than in the composite materials, even at the much higher stress levels used to test the composites. Neutral-plane migration in the matrix bars was confirmed through a limited number of tests using the technique of pairing double vertical rows of indentations [9]. The neutral-plane migration measured was slightly greater than that calculated using the above analysis.

The driving force for neutral-plane migration is stress redistribution across the bar due to unequal creep rates in tension and compression. From Equation 1 and the numerically determined creep parameters, the tensile and compressive steady-state stress distributions may be calculated for each set of test

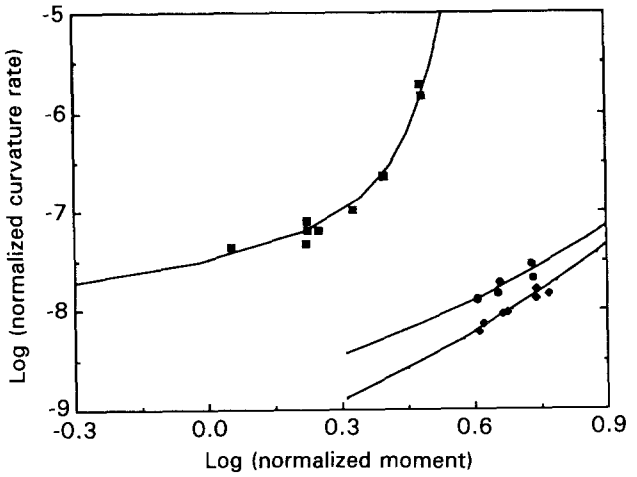

Figure 3 Numerical solution of the stress dependence for monolithic Si_3N_4 and composites at 1200 °C plotted as normalized curvature rate as a function of applied moment: (■) matrix, (◆) 20 vol %, (●) 30 vol %, (——) best fits.

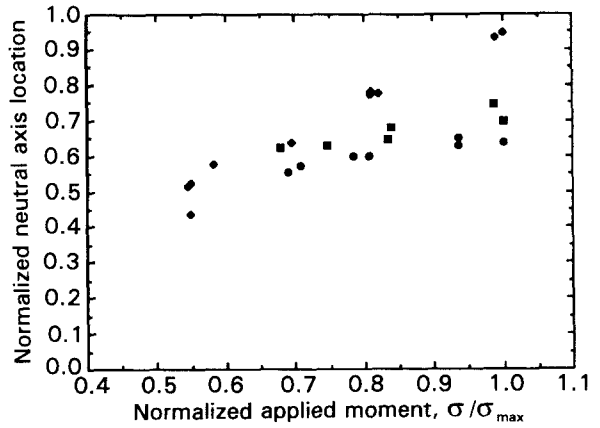

Figure 4 Normalized neutral-plane location (0.0 = tensile surface) versus applied stress for all materials as determined from numerical solutions: (◆) matrix, (●) 20 vol %, (■) 30 vol %.

conditions. Stress distributions in crept specimens are shown for each material in Figs 5–7.

3.3. Effect of neutral-plane migration

The creep strain shown in Fig. 1 was calculated directly from the measured deflections assuming no migration of the neutral plane using [12]

$$\varepsilon = \frac{4H}{l^2} U_{cp} \quad (3)$$

Here ε is the strain, U_{cp} the deflection of the centre point relative to the load points, l the length of the inner span and H the thickness. Calculating the strain from the measured deflections using Equation 3 requires two assumptions: (i) that neutral planes remain at the centroid and (ii) that plane sections of the creeping bar remain plane in bending. The second assumption is part of Chuang's analysis for stress dependence [8], but the stress redistribution and neutral-plane migration accommodated by this analysis violate the first assumption. Neutral-plane migration has been observed in SiAlON [4, 9] and the current Si_3N_4 matrix bars. Calculation of true strains involves a correction of the strains calculated using Equation 3.

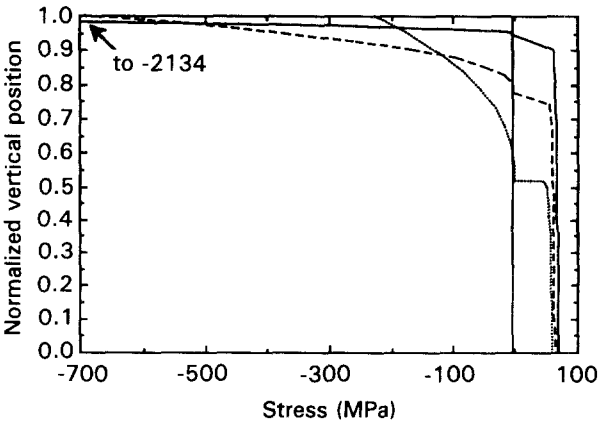

Figure 5 Compressive and tensile steady-state stress distributions for monolithic Si_3N_4 at 1200 °C and stresses of (. . .) 100, (– – –) 150 and (——) 185 MPa.

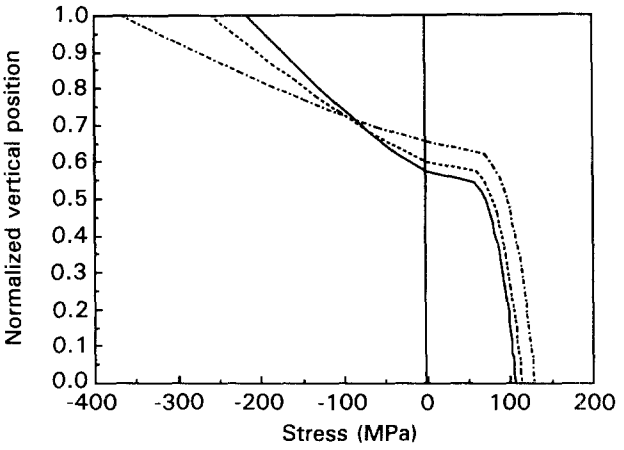

Figure 6 Compressive and tensile steady-state stress distributions for 20 vol % composite at 1200 °C and stresses of (——) 250, (– – –) 280 and (—.—) 330 MPa.

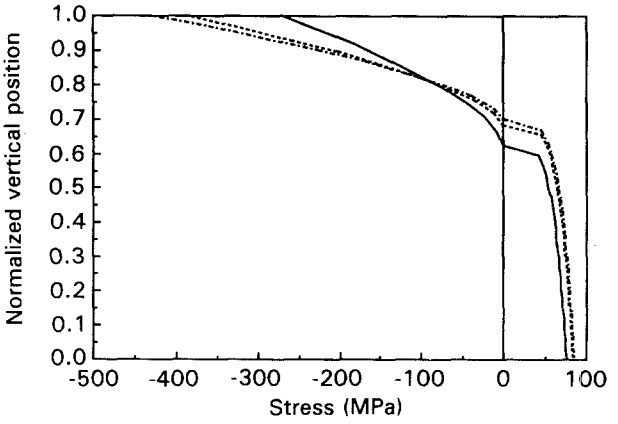

Figure 7 Compressive and tensile steady-state stress distributions for 30 vol % composite at 1200 °C and stresses of (——) 250, (– – –) 280 and (—.—) 330 MPa.

Because the strain exhibits a linear distribution in the bar even after neutral-plane shifting, the true strain will be directly proportional to the magnitude of the shift. As shown in Fig. 8, the true strain at any given time will be the strain calculated from Equation 2, corrected by a factor of $H_t/0.5$ that varies as $1 \leq H_t/0.5 < 2$, a factor of 2 being the physically impossible situation of having a compressive zone with zero thickness.

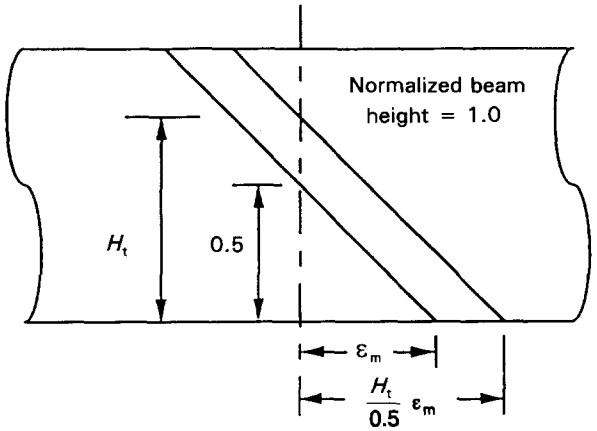

Figure 8 Geometry of the creep strain correction due to neutral-plane shifting during flexural creep.

The initial solution set of NPC was used to calculate strain rates which were then refitted, generating a new set of NPC and power-law parameters. Multiple iterations were performed until the analysis converged to a single consistent set of steady-state NPC, power-law creep parameters and corrected strain-rates. The surprising result was that adjustments in the set of power-law stress parameters to account for the corrected strain rates were less than 1% for any of the materials. To estimate the strain rates at higher temperatures, correction factors for stress-dependent strain rates and shifts in NPC were correlated and matched to the high-temperature data. A maximum 10% increase in activation energy was found for the composites, while a maximum increase of 16% was found for the unreinforced matrix. The uncorrected [7] and corrected activation energy for the matrix and composites are listed in Table II.

TABLE II Uncorrected and corrected activation energies for the monolithic matrix and components

	Activation energy (kJ mol^{-1})	
Material	Uncorrected	Corrected
Matrix	530	619
20 vol % composite	390	428
30 vol % composite	371	407

4. Discussion

4.1. Stress distribution evolution and neutral-plane migration

The simultaneous tensile and compressive deformation in a bar during flexural creep result in complex transient creep stages. Investigators of flexural creep in ceramics have reported both the exsistence and the absence of a steady-state creep stage [13, 14]. When a steady-state strain rate is observed, the transient or primary creep stage in flexural creep is found to persist to much longer times and greater strains when compared with uniaxial tensile or compressive creep tests under similar conditions. Chuang *et al.* [15] considered that the prolonged transient creep period was due to stress relaxation, with the change in stress expressed as

$$d\sigma = \left.\frac{\partial\sigma}{\partial t}\right|_{\varepsilon} dt + \left.\frac{\partial\sigma}{\partial\varepsilon}\right|_{t} d\varepsilon \qquad (5)$$

This equation describes two contributing processes, (i) stress relaxation through creep flow due to an imposed strain and (ii) production of elastic stress caused by increasing strain. The rate at which stresses are redistributed within the bar will depend on the tensile and compressive creep rates of the material. If the rates are identical, lateral force equilibrium is maintained even during stress relaxation and no migration of the neutral plane occurs. When creep deformation proceeds faster in tension than in compression, the tensile load capacity is reduced and the stress distribution requires an enlarged tensile zone to maintain force equilibrium. This phenomenon is manifested as neutral-plane migration [15, 16].

Redistribution of the stress in the beam continuously evolves with time until a steady state is reached [15]. Steady-state stress distributions are shown in Figs 5–7 for the matrix and composite materials. Two important features of these stress distributions are the high shear stresses close to the neutral axis and the approximately constant stress level throughout the tensile stress zones. Horizontal cracks (parallel to the length of the bar) occurring in the matrix bars are direct evidence for such large shear stresses [7]. Observation of shear cracks at different vertical positions of the bar indicates shifting of the neutral plane during deformation. Formation of Mode I cracks has been observed at the tensile surface perpendicular to the tensile stress direction and to the shear-type cracks [7]. For all materials tested, the maximum steady-state tensile stress is calculated to be less than half of the initially applied elastic stress. Tensile stress relaxation in flexural creep has been reported previously [16, 17]. Chuang *et al.* [15] found that the maximum stress in the outer material plane decayed very quickly compared with the time needed for complete evolution of the steady-state stress distribution. This may account for the excellent creep resistance in the composites, even at stresses that are 80–90 % of the ultimate strength [2]. If a strength-limiting surface flaw is not severe enough to cause immediate rupture, the stress intensity may decay too quickly for it to grow to a critical size.

Tensile stress relaxation and the accompanying stress redistribution is observed in the composites. From the composite creep strains in Fig. 1, stresses were calculated via the fibre compliance [18] and plotted against time for the 20 vol % composite tested at 1200 °C/250 MPa. This result is shown in Fig. 9. As shown, the stress relaxed from an initial value of ~ 1050 MPa to 500 MPa at the steady state. Assuming that the initial 250 MPa load in the composite is completely supported by the fibre volume fraction, the stress in the fibres is calculated to be 1250 MPa. This value agrees very well with the fibre stresses calculated from the composite creep strains and the fibre compliance. Such initially high fibre stress is evidence that substantial relaxation is occurring in the matrix phase. To assess the relative stress relaxation in the fibres when the steady state is reached, the tensile zone stress

distribution (Fig. 6) was used to calculate the maximum fibre stress. If the fibres sustain the whole tensile load, a stress of 550 MPa is calculated. Again, this value is consistent with that calculated from the strain and fibre compliance, if the load is mainly supported by the fibres. The curve in Fig. 9 suggests that transient creep response as well as the stress redistribution is dominated by the reinforcing fibres.

TABLE III Primary creep stress exponent as a function of time for unreinforced Si_3N_4

Time (h)	n_p
0.1	5.7
0.33	4.7
1.0	3.0
10.0	2.6

4.2. Stress exponents

The compressive stress exponents are 1.1 and 0.7 for the 20 and 30 vol % composite materials, respectively. In amorphous grain-boundary phase materials, such as the matrix, compressive stress exponents of the order of unity have previously been associated with Coble creep where material diffusion is dominant along the grain boundaries [5, 19]. Exponents of unity have also been correlated with viscous flow of the grain boundary phase [20]. For the SCS-6 fibre compressive creep data are not yet available. An n_c of 2.3 was obtained by Carter *et al.* [20] for bulk CVD SiC for which the creep mechanism was determined to be dislocation glide. The rate-controlling step was overcoming the Peierls stresses. The activation energy, though, reported as 173 kJ mol^{-1} between 1673 and 1873 K and at a stress of 220 MPa, is too low to account for the rate-controlling mechanism in the current composite materials. This means that dislocation glide in the fibres is possible at 1200 °C, but the {1 1 1} planes on which dislocations are most likely to move are oriented parallel to the fibre axis, minimizing the resolved shear stress on the {1 1 1} planes and hence the dislocation motion. However, axially oriented shear stresses generated during load transfer may cause limited dislocation activity. Compressive creep stress exponents of the order of unity for the composites might be associated with diffusive or viscous flow mechanisms in the matrix phase. The fibre will have an effect on this parameter, though to what extent it is not known.

The tensile creep stress exponent for the matrix data is 22, which is significantly higher than that of 5 for the composites. Chen and Chuang [9] reported a tensile creep stress exponent of 13.8 for an SiAlON material using the same numerical procedure. They attributed this high tensile creep stress exponent to a diffusive creep crack growth mechanism. High-temperature subcritical-crack growth exponents up to 40 have been reported, [21]. Khandelwal *et al.* [22] reported an n_{cg} of 22 for 6 wt % Y_2O_3–2 wt % Al_2O_3–Si_3N_4, and observed slow crack growth occurring within the intergranular phase by grain boundary sliding, cavitation, and cavity linkage. Microstructural examination of crept matrix specimens in the current study confirmed that intergranular microcrack growth occurred.

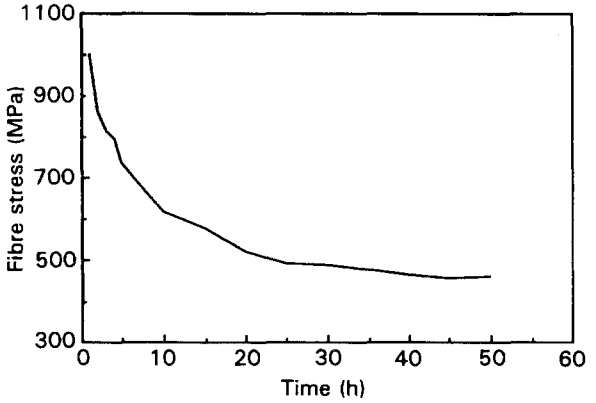

Figure 9 Fibre stresses calculated using the compliance method of DiCarlo [16], plotted against time for the 20 vol % composite tested at 1200 °C/250 MPa.

Reinforcing the Si_3N_4 with SiC fibres reduces the tensile stress exponent from 22 to 5, indicating both a reduced susceptibility to matrix subcritical crack nucleation and growth and a change in the creep mechanism. The tensile stress exponent determined numerically is in good agreement with experimental results ($n_t = 6$) [23]. Since the stress exponent for the SCS-6 fibres up to 1400 °C at 278 MPa is unity [18], the stress dependence exhibited by the composites would appear to originate from another source. The stresses in the fibres, though, are calculated to have been much greater in these creep tests than in the single-filament tests of DiCarlo [16]. In view of the periodically repeating stress relaxation postulated to occur within the composites [7], one explanation might be that the stress exponent is associated with a primary or transient creep process in the *matrix* phase. In an analysis of flexural creep of hot-pressed MgO–Si_3N_4, Fett *et al.* [24], using creep strains measured at 0.1 h, reported a primary creep stress exponents of 5.6. Using their analysis procedure based on strain at constant time, primary creep stress exponents for the matrix Si_3N_4 were calculated and are tabulated in Table III. This analysis assumes negligible creep asymmetry within the bar at such short times. However, initial stresses within a creeping Si–SiC bar were previously found to decay very rapidly and render the above assumption invalid [16]. The assumption of negligible creep asymmetry, though, was shown to be non-critical in the general stress analysis. After accounting for creep asymmetry (neutral-plane migration), the stress parameters changed by less than 1 % if at all, even reaching a steady state. The consistency between the stress exponents for primary creep (~ 0.3 h) in the matrix and steady-state creep in the composites suggests that there is a continuously changing stress distribution in the matrix phase of the composites. The sharp fall-off in primary stress exponent with time would also suggest a relaxation time of ~ 0.3 h for a stress wave or redistribution. If correct, this also implies a cyclical creep mechanism as proposed previously [7]. Though

inconclusive, these arguments show that the creep mechanism in the composites may not easily be assigned to a simple mechanism.

4.3. Activation energy

The unreinforced matrix under an applied stress of 100 MPa exhibited an apparent activation energy (532 kJ mol^{-1} over the 1200–1350 °C temperature range. When calculated using the estimated strain rates, an activation energy of 619 kJ mol^{-1} is obtained. The corrected value is consistent with the activation energies of ~ 650 kJ mol^{-1} tabulated by Davis and Carter [17] for several hot-pressed silicon nitrides having various amounts and compositions of sintering additives. It is also in the range of activation energies for which Birch *et al.* [25] proposed that creep is governed by the rate of *microcrack* formation within the intergranular phase.

Apparent activation energies for the 20 and 30 vol % fibre composites were calculated as 390 kJ mol^{-1} at 250 MPa/1200–1350 °C and 370 kJ mol^{-1} at 250 MPa/1200–1450 °C, respectively. Values calculated from estimated strain rates were 428 and 407 kJ mol^{-1}. Because these energies are approximately equivalent, the same creep deformation mechanism is assumed to be operative. Both activation energies are lower than that determined for the unreinforced matrix and that of 480 kJ mol^{-1} determined for the SiC fibre [18] (the only data available). In a previous study [26] it was reported that at temperatures below 1823 K, Si–N diffusion in the grain boundary phase of Y_2O_3–Si_3N_4 had an activation energy of 448 kJ mol^{-1}. This is quite close to the measured activation energies, considering the possible impurity content and fabrication differences [26, 27]. The possibility that the composite activation energies (407 and 428 kJ mol^{-1}) are dictated by the intergranular phase would seem to conflict with the activation energy (619 kJ mol^{-1}) measured for the matrix, but the stress state within the matrix phase of the composites is much different to that in the matrix bars. Also, it was presumed that the creep mechanism for a given material was the same over all temperature and stress levels. Changes in mechanism from non-cavitational to cavitational have been observed in Si_3N_4 and Si–SiC ceramics when tested over sufficiently high stress and temperature ranges [16, 20, 28]. For the current matrix material there may be a threshold stress below which microcrack formation does not control the creep mechanism. The stress of 100 MPa used to determine the activation energy of the current Si_3N_4 was found to generate intergranular crack formation and is obviously over this threshold. Through the restraining force supplied by the composite reinforcing fibres, the matrix phase stresses may never reach the microcracking threshold, or because of the temporal nature of creep, the threshold may be reached only transiently such that sufficient stress intensity is not maintained for microcrack formation. Without the imposition of microcracking, matrix creep would be controlled by the properties of the intergranular phase. This also suggests that if measured at sufficiently low stresses the activation energy of the matrix would be that of the composites between 1200 and 1350 °C.

5. Conclusions

The tensile stress exponent determined using the model proposed by Chuang is in close agreement with experimental results. The proposed deformation mechanism was supported by the fact that the steady-state stress exponent is consistent with the stress exponents for primary creep in the matrix material, yet the creep strain curves are clearly dominated by creep of the SiC fibre. The corrected activation energies for the composites appear to correspond with the activation energy measured for Si–N diffusion through the grain boundary phase. While long-term composite creep strains are controlled by deformation in the reinforcing fibre, the stress dependence and deformation kinetics appear to be dictated by the matrix phase. Further research will be needed to verify the proposed rate-controlling mechanisms.

Acknowledgements

This work was partially supported by the National Science Foundation (MSS 9057030). We are grateful to Dr T.-J. Chung at the National Institute of Standard and Technology for helpful discussion.

Appendix: Numerical stress analysis

Incorporating Equation 2 into the force and moment balance calculations for a bar in four-point bending creep resulted in two governing equations [9]. From the force balance

$$\left[\frac{A^{(1/n_t+1)}}{A_c^{[n_t/n_c(n_t+1)]}}\dot{k}^{(n_t-n_c)/[n_c(n_t+1)]}\left(\frac{\dot{n}_c(n_t+1)}{n_t(n_c+1)}\right)^{n_t/(n_t+1)}\right] h_c^{n_t(n_c+1)/[n_c(n_t+1)]} + h_c - 1 = 0 \quad \text{(A1)}$$

From the moment balance

$$\left(\frac{\dot{k}}{A_t}\right)^{1/n_t}\frac{n_t}{2n_t+1}(1-h_c)^{(2n_t+1)/n_t} + \left(\frac{\dot{k}}{A_c}\right)^{1/n_c} n_c/2n_c + 1\, h_c^{(2n_c+1)/n_c} = m \quad \text{(A2)}$$

A single data point consisted of the normalized curvature rate, $\dot{k}$, the normalized moment, m, and the normalized neutral plane distance from the compressive stress surface, h_c. At an applied stress σ, $m = \sigma/6$ and $\dot{k} = 2\dot{\varepsilon}$ [20]. Because an analytic solution for these equations does not exist, a numerical method is employed. First, reasonable values for the creep parameters A_t, n_t, A_c and n_c are chosen, and then for each value of $\dot{k}$ a corresponding neutral axis location h_c is found using Equation A1 through a Newton–Ralphson root-finding algorithm. Non-linear regression is then used to fit Equation A2 to the three one-dimensional arrays of $\dot{k}$, h_c and applied stress m. The analysis is then restarted using the numerically determined parameters A_t, n_t, A_c and n_c. The best estimate of the creep parameters A_t, n_t, A_c and n_c is obtained

when a self-consistent parameter set is determined, i.e. when h_c does not change on the following iteration.

References

1. J. J. MECHOLSKY, *Ceram. Bull.* **68** (1989) 367.
2. J.-M. YANG, S. T. CHEN, R. B. THAYER and J.-F. LeCOSTAOUEC, *J. Mater. Res.* **6** (1991) 1926.
3. S. M. WIEDERHORN, D. E. ROBERTS, T.-J. CHUANG and L. CHUCK, *J. Amer. Ceram. Soc.* **71** (1988) 602.
4. M. K. FERBER, M. G. JENKINS and V. J. TENNERY, *Ceram. Eng. Sci. Proc.* **8** (1987) 778.
5. W. R. CANNON and T. G. LANGDON, *J. Mater. Sci.* **23** (1988) 1.
6. J.-M. YANG, R. B. THAYER, S. T. CHENA and W. LIN, in Proceedings of ICCM VIII, 1991, edited by S. W. Tsai and G. S. Springer (SAMPE, Covina, CA, 1991) p. 23-C.
7. R. B. THAYER and J.-M. YANG, *Mater Sci. Engng* **A160** (1993) 169.
8. T.-J. CHUANG, *J. Mater. Sci.* **21** (1986) 165.
9. C.-F. CHEN and T.-J. CHUANG, *J. Amer. Ceram. Soc.* **73** (1990) 2366.
10. F. ABBE, R. CARIN and J.-L. CHERMANT, *J. Eur. Ceram. Soc.* **5** (1989) 201.
11. F. H. NORTON, "Creep of Steel at High Temperatures" (McGraw-Hill, New York, 1929) p. 67.
12. G. W. HOLLENBERG, G. R. TERWILLINGER, and R. S. GRORDON, *J. Amer. Ceram. Soc.* **54** (1971) 196.
13. U. ERNSTBERGER, G. GRATHWOHL and F. THUMMLER, in Proceedings of 2nd International Symposium on Ceramic Materials and Components for Engines, edited by E. W. BUNK, H. HAUSNER and B. HONNET (American Ceramic Society, Westerville, OH, 1986) p. 485.
14. T.-J. CHUANG and S. M. WIEDERHORN, *J. Amer. Ceram. Soc.* **71** (1988) 595.
15. T.-J. CHUANG, S. M. WIEDERHORN and C.-F. CHEN, in "Creep and Fracture of Engineering Materials and Structures," edited by B. WILSHIRE and R. W. EVANS (Institute of Metals, London, 1987) p. 957.
16. J. A. DICARLO, *J. Mater. Sci.* **21** (1986) 217.
17. R.F. DAVIS and C. H. CARTER Jr, in "Advanced Ceramics, editor-in-chief S. Saito (Oxford University Press, Oxford, 1988) p. 95.
18. F. F. LANGE and B. I. DAVIS, *J. Mater. Sci.* **17** (1982) 3637.
19. M. K. BRUN and M. P. BOROM, *J. Amer. Ceram. Soc.* **72** (1989) 993.
20. C. H. CARTER Jr, R. F. DAVIS and J. BENTLEY, *ibid.* **67** (1984) 732.
21. B. S. B. KARUNARANTE and M. H. LEWIS *J. Mater. Sci.* **15** (1980) 449.
22. P. K. KHANDELWAL, J. CHANG and P. W. HEITMAN, in Fracture Mechanics of Cermaics, Vol. 8. Edited by R. C. Bradt, A. G. Evans, D. P. H. Hasselman and F. F. Lange (Plenum, New York, 1986).
23. J. W. HOLMS, *J. Mater. Sci.* **26** (1991) 1808.
24. T. FETT, K. KELLER and D. MUNZ, *ibid.* **23** (1988) 467.
25. J. M. BIRCH, B. WILSHIRE, D. J. R. OWEN, and D. SHANTARAM, *ibid.* **11** (1976) 1817.
26. R. E. LOEHMAN, *J. Amer. Ceram. Soc.* **62** (1979) 491.
27. R. A. L. DREW, S. HAMPSHIRE and K. H. JACK, in "Progress in Nitrogen Ceramics," edited by F. L. RILEY (Martinus Nijhoff, Boston 1983) p. 323.
28. R. D. NIXON, D. A. KOESTER, S. CHEVACHAROENKUL and R. F. DAVIS, *Compos. Sci. Tech.* **37** (1990) 313.

Received 3 September 1992
and accepted 5 July 1993